4018–4027 *Nucleic Acids Research, 1997, Vol. 25, No. 20*

Isoalloxazine derivatives promote photocleavage of natural RNAs at G·U base pairs embedded within helices

Petra Burgstaller[+], Thomas Hermann[1], Christian Huber, Eric Westhof[1] and Michael Famulok*

Institut für Biochemie der LMU München-Genzentrum, Würmtalstraße 221, 81375 München, Germany and [1]Institut de Biologie Moléculaire et Cellulaire, CNRS UPR SMBMR, 15 Rue Rene Descartes, 67084 Strasbourg Cedex, France

Received July 16, 1997; Revised and Accepted August 26, 1997

ABSTRACT

We have recently shown that isoalloxazine derivatives are able to photocleave RNA specifically at G·U base pairs embedded within a helical stack. The reaction involves the selective molecular recognition of G·U base pairs by the isoalloxazine ring and the removal of one nucleoside downstream of the uracil residue. Divalent metal ions are absolutely required for cleavage. Here we extend our studies to complex natural RNA molecules with known secondary and tertiary structures, such as tRNAs and a group I intron (td). G·U pairs were cleaved in accordance with the phylogenetically and experimentally derived secondary and tertiary structures. Tandem G·U pairs or certain G·U pairs located at a helix extremity were not affected. These new cleavage data, together with the RNA crystal structure, allowed us to perform molecular dynamics simulations to provide a structural basis for the observed specificity. We present a stable structural model for the ternary complex of the G·U-containing helical stack, the isoalloxazine molecule and a metal ion. This model provides significant new insight into several aspects of the cleavage phenomenon, mechanism and specificity for G·U pairs. Our study shows that in large natural RNAs a secondary structure motif made of an unusual base pair can be recognized and cleaved with high specificity by a low molecular weight molecule. This photocleavage reaction thus opens up the possibility of probing the accessibility of G·U base pairs, which are endowed with specific structural and functional roles in numerous structured and catalytic RNAs and interactions of RNA with proteins, in folded RNAs.

INTRODUCTION

Certain organic compounds of low molecular weight, designated photosensitizers, can damage biomolecules upon irradiation with light. Endogenous photosensitizers such as porphyrins and flavins might be involved in photocarcinogenesis because their reaction products may lead to misreplication of DNA, mutations and cancer (1). Natural and synthetic photosensitizers have attracted considerable interest because of their utilization in photochemotherapy, the treatment of diseases with photosensitizing drugs plus light (2). Another important application of photochemotherapy is the treatment of tumors with photosensitizers like hematophorphyrin (3). Photosensitizers have also been applied to the inactivation of viruses in contaminated medical samples such as blood plasma (4).

The isoalloxazine derivative riboflavin can promote photooxidative strand scission in DNA after treatment with piperidine by generating 8-hydroxydeoxyguanosine (5–7). An artificial restriction endonuclease was obtained as a synthetic netropsin–flavin hybrid molecule which cleaves DNA at a specific A:T-rich locus determined by the sequence specificity of the netropsin moiety (8). In contrast to DNA, however, little is known about the effect of photosensitizers on RNA.

Recently we isolated an RNA aptamer by *in vitro* selection that specifically recognizes the isoalloxazine moiety of FMN or FAD in solution (9). During the structural characterization of this aptamer we observed that isoalloxazine derivatives (Fig. 1) can induce strand breakage 3′ of the uracil of G·U wobble base pairs by a photooxidative cleavage mechanism (10). Strand breakage also occurred with high specificity in a variant of this RNA aptamer lacking the FMN binding site while still containing the G·U pairs embedded within a helix. Thus, the photocleavage reaction did not require a high affinity FMN or isoalloxazine binding site in the RNA. Furthermore, no bias for the removed nucleoside exists, as cleavage occurs independently of the residue located 3′ of the uracil involved in G·U base pairing (10).

Here we have investigated the specificity and applicability of isoalloxazine-induced photocleavage for recognition of G·U base pairs in large folded RNAs by testing biologically relevant RNAs with known tertiary structures (11–15), such as yeast $tRNA^{Phe}$, $tRNA^{fMet}$, $tRNA^{Asp}$ and $tRNA^{Val}$. In addition, to test the potential of isoalloxazines as specific structure probes for G·U wobble

[+]Present address: Department of Chemistry, University of Florida, PO Box 117200, Gainesville, FL 32611-7200, USA

*To whom correspondence should be addressed. Tel: +49 89 74017 410; Fax: +49 89 74017 448; Email: Famulok@lmb.uni-muenchen.de

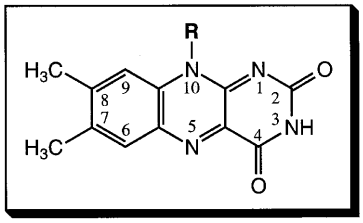

R = CH_3: Lumiflavin

D-*ribo*-2,3,4,5-tetrahydroxypentyl: riboflavin

D-*ribo*-2,3,4-trihydroxypentyl-5-phosphate ester: FMN

Figure 1. Chemical structures of isoalloxazine derivatives used for photo-induced RNA cleavage.

pairs in larger biologically functional RNAs, we applied this method to map the G·U base pairing scheme in a group I self-splicing intron, the td intron in the precursor RNA for phage T4-derived thymidylate synthase mRNA (16). G·U pairs were affected in accordance with a previously refined model of the intron structure (17). Based on crystallographic data on $tRNA^{Asp}$ we performed molecular dynamics simulations of a ternary complex of the G·U-containing helix, FMN and a divalent metal ion. The simulations provide a rationale for the observed cleavage specificity. These results thus open the exciting possibility of using isoalloxazines as highly specific structure probes for G·U base pairs in RNA molecules.

Highly conserved G·U wobble base pairs are present in many natural RNAs such as group I and group II ribozymes (18–22), tRNAs (23), the spliceosome (24) and 16S and 23S rRNAs (25) and were often found to be functionally important (18–26). G·U pairs are also implicated in RNA–protein recognition. For example, in recognition of *Escherichia coli* $tRNA^{Ala}$ by alanyl-tRNA synthetase a G·U pair in the acceptor stem of the tRNA is critical in determining $tRNA^{Ala}$ acceptor identity (23,26). Given their biological importance, it would be highly desirable to directly probe RNA structures for the existence and accessibility of wobble and other non-canonical base pairs. To date, however, no suitable probe for specific recognition and direct detection of unusual base pairs in RNA molecules has been reported. This study describes such specific activity in structural probing of folded RNAs and, in addition, explains the specificity at the structural level.

MATERIALS AND METHODS

Materials

Riboflavin, FMN, FAD, lumiflavin and lumichrome were purchased from Fluka, [γ-^{32}P]ATP and [5′-^{32}P]pCp from Amersham. Yeast $tRNA^{Phe}$, $tRNA^{fMet}$ and $tRNA^{Val}$ were obtained from Sigma, yeast $tRNA^{Asp}$ was a generous gift from Dr G.Keith (Strasbourg). Plasmid td ΔP6-2T containing 100 nt of the 5′ exon, the 265 nt td intron and 56 nt of the 3′ exon were generous gifts from Dr R.Schroeder (Biocenter Vienna) (27). T7 RNA polymerase was purified from the overproducing strain BL21/pAR1219, following the purification protocol provided by F.W.Studier (28). DNase I (RNase-free) was from Boehringer Mannheim, Taq polymerase from Eurogentec and T4 polynucleotide kinase, T4 RNA ligase and calf intestinal alkaline phosphatase from New England Biolabs. Ultrapure, unlabeled NTPs and dNTPs were obtained from Boehringer Mannheim. Primers and synthetic oligonucleotides used in PCR amplification reactions were synthesized on a Millipore Expedite oligonucleotide synthesizer using standard phosphoramidite chemistry. Oligonucleotides were purified as described previously (29) and concentrations were determined by absorbance measurements at 260 and 280 nm.

Preparation of DNA and RNA

The RNAs used for this study were transcribed from DNA templates containing a T7 promotor. DNA templates were generated by PCR amplification of synthetic oligonucleotides. PCR reactions were performed in PCR buffer (10 mM Tris–HCl, pH 8.3, 50 mM KCl, 0.001% gelatin, 1.5 mM $MgCl_2$, 0.3% Tween 20, 0.2 mM dNTPs) in the presence of 3 mM primer and 2 U Taq polymerase. The precursor RNA of the T4 phage-derived thymidylate synthase (td) intron was *in vitro* transcribed from plasmid td ΔP6-2T containing 100 nt of the 5′ exon, the 265 nt intron and 56 nt of the 3′-exon (30). Aliquots of 250 nM precursor RNA were pre-incubated and renatured as described previously (27,31).

RNA labeling

For 5′-end-labeling the transcribed RNA was dissolved in CIP buffer (50 mM Tris, pH 8.5, 0.1 mM EDTA, 0.1 mg/ml BSA) and treated with 0.05 U/pmol RNA calf intestinal alkaline phosphatase for 30 min at 37°C. After purification by preparative gel electrophoresis on polyacrylamide–8.3 M urea gels, ~10 pmol eluted RNA was redissolved in kinase buffer (70 mM Tris–HCl, pH 7.6, 10 mM $MgCl_2$, 5 mM DTT), 5′-end-labeled using 10 U T4 polynucleotide kinase and 30 mCi [γ-^{32}P]ATP for 30 min at 37°C and again purified on polyacrylamide–8.3 M urea gels. For 3′-labeling 30 pmol RNA was incubated with 30 mCi [5′-^{32}P]pCp in 50 mM HEPES, pH 7.5, 20 mM $MgCl_2$ in the presence of 6 U T4 RNA ligase at 4°C for 12–16 h followed by gel purification.

Flavin cleavage experiments

Reactions were performed in Eppendorf tubes in a total volume of 20 µl. Aliquots of 250 nM 5′-^{32}P-end-labeled RNA (~10 000 c.p.m.) were denatured in 200 mM NaCl, 50 mM Tris–HCl, pH 7.6, 2 mM EDTA for 3 min at 95°C and subsequently renatured for 10 min at room temperature. After adding $MgCl_2$ to a final concentration of 12 mM, the RNA was irradidated in the presence of 200 µM FMN or riboflavin (100 µM for lumiflavin; see Fig. 5) at ambient temperature for up to 4 h using incident light from a polychromatic lamp (20 J/s) at a distance of between 25 and 30 cm from the RNA sample. Light irradiation had no detectable effect on the temperature of the RNA samples. The reaction was stopped by precipitation by addition of 60 µl ethanol. The RNA was redissolved in H_2O and analyzed on polyacrylamide–8.3 M urea gels. For calibration of gel band positions 5′-labeled RNA was cleaved at G residues by digestion with T1 ribonuclease or was subjected to alkaline hydrolysis, as described elsewhere (32). For hydroxyl radical cleavage the RNA was incubated in 1 mM $Fe(NH_4)_2(SO_4)_2 \cdot 6H_2O$, 2 mM EDTA, 0.05% H_2O_2, 5 mM DTT at 25°C for 10 min (33,34).

Flavin cleavage in the absence of oxygen

All buffers and stock solutions used for cleavage experiments in the absence of oxygen were degassed for 1 h by ultrasonication

in the presence of argon. Subsequently, a stream of argon was bubbled through the solvents and buffers for 15 min. These two steps were repeated at least once. Bottles were sealed with rubber caps and solutions removed with tight sealing, argon-rinsed syringes in a stream of argon. Reactions were performed in sealed tubes which were rinsed with argon for at least 15 min. During pipetting of the solutions and during incubation, care was taken to avoid oxygen contact by applying an argon blanket. Reactions were performed in the same way as described above.

Molecular modeling and simulations

Coordinates for the RNA were taken from the crystal structure of yeast $tRNA^{Asp}$ (nt U_1–A_7 paired to nt U_{66}–A_{72}; 15), coordinates for FMN were from a molecular model constructed with the Insight program (Biosym Technologies, San Diego). Docking of the FMN molecule to the RNA helix was done manually, accounting for the probable hydrogen bonding interactions of the isoalloxazine ring with the amino group of the G of the G·U pair and the 2′-OH of the U. The conformation of the FMN exocyclic sugar moiety was chosen in such a way that no interaction of the sugar with the RNA occurred. A Mg^{2+} ion was placed manually, bridging an exocyclic carbonyl oxygen of the isoalloxazine moiety and the phosphate of the nucleotide 3′ of the U of the G·U pair.

For molecular dynamics simulations the AMBER 4.1 (35) package was used. Forcefield parameters for FMN were derived as described previously (36). Parameters for Mg^{2+} were from Åqvist (37). The RNA was placed in a rectangular box of SPC/E water containing about 2500 solvent molecules. Eleven Na^+ counterions were placed according to the electrostatic potential around the solute such that no ion was closer than 4.5 Å to any solute atom. The simulations were run with a time step of 2 fs at a constant temperature of 298 K and a constant pressure of 1 atm. The SHAKE algorithm was used to constrain the X-H bond lengths. Van der Waals interactions were truncated at 9.0 Å, while no cut-off was applied to the electrostatic term. The electrostatic interactions were calculated by the Particle Mesh Ewald method with a charge grid spacing close to 1.0 Å. The equilibration protocol was similar to those used in preceding work (38,39).

RESULTS AND DISCUSSION

Cleavage is specific for G·U pairs

Natural RNAs with a known secondary and tertiary structure and without known specific affinity for flavins were chosen in order to demonstrate that photoinduced cleavage of RNA by isoalloxazines is a general phenomenon. We first tested a series of transfer RNAs: $tRNA^{Phe}$, $tRNA^{fMet}$, $tRNA^{Val}$ and $tRNA^{Asp}$. Yeast $tRNA^{Phe}$ contains a single G·U wobble base pair in the acceptor stem, G4·U69 (Fig. 2A). Accordingly, with 5′-end-labeled $tRNA^{Phe}$ a single cleavage signal at U69 was obtained (10). Analogously, $tRNA^{fMet}$ and $tRNA^{Val}$, which contain, respectively, a U51·G65 and G50·U64 pair in the T stem, showed a corresponding single cleavage signal at U51 and U64 (Fig. 2B and C). No other position was affected by the photosensitizer in these tRNA molecules.

$tRNA^{Asp}$ contains three G·U base pairs (U5·G68, G10·U25 and G30·U40) and one structurally equivalent Ψ13·G22 base pair. The effects of irradiation of 3′-end-labeled $tRNA^{Asp}$ incubated with 200 µM FMN for 1 h with visible light are shown in Figure 2D. A major cleavage signal was obtained for U5·G68 and a weak band was observed at G30·U40. No cleavage was detected at the G10·U25 and the G22·Ψ13 base pairs, both of which flank the D helix.

No preference for the removed nucleoside

In the tRNAs described so far the nucleoside removed downstream of the uracil of the cleaved G·U base pair was either a guanosine or a cytosine. We therefore analyzed several synthetic RNA constructs with different residues located 3′ of the uracil to test whether a bias for the nucleoside removed exists. In addition, RNA constructs containing tandem G·U pairs or a U·U mismatch adjacent to the G·U pairs were tested. As summarized in Table 1, only the RNA which contained two G·U pairs in tandem alignment was not cleaved (Table 1, row 6). In all other constructs cleavage occurred independently of the residue located 3′ of the uracil involved in G·U base pairing.

Table 1. FMN-dependent cleavage of different synthetic and natural RNAs

RNA	Length (nt)	G·U-containing stem	Residue 3′ of U	Intensity[a]	Row[a]
FMN-2	109	5′-CCGAC**U**GUGGU	G	++	1
		3′-GGCUG**G**CACCA			
PB-5	107	5′-U**G**CUC	A	+	2
		3′-A**U**GAG			
PB-7	113	5′-CU**U**C	C	++	3
		3′-GA**G**G			
PB-13	110	5′-CUUCACU–**G**CA**U**U_1CC	U_1	+	4
		3′-GAAGUGU_2**U**GU**G**A–GG	U_2	++	
PB-9	74	5′-CGC**G**CC	G	++	5
		3′-GCG**U**GG			
PB-5/2	107	5′-**GG**AGCC	U	–	6
		3′-A**UU**UCGG	A	–	

[a]++, strong cut; +, medium to weak cut; –, no cut.

[b]Row 1, example of a strong cut when G is removed; row 2, example of a cut when A is removed; row 3, example of a strong cut when C is removed; row 4, example of a cut when U1 is removed and example of a cut when U2 belonging to a U-U mismatch is removed; row 5, example of a strong cut when G is removed; row 6, no cleavage detectable at tandem G·U pairs.

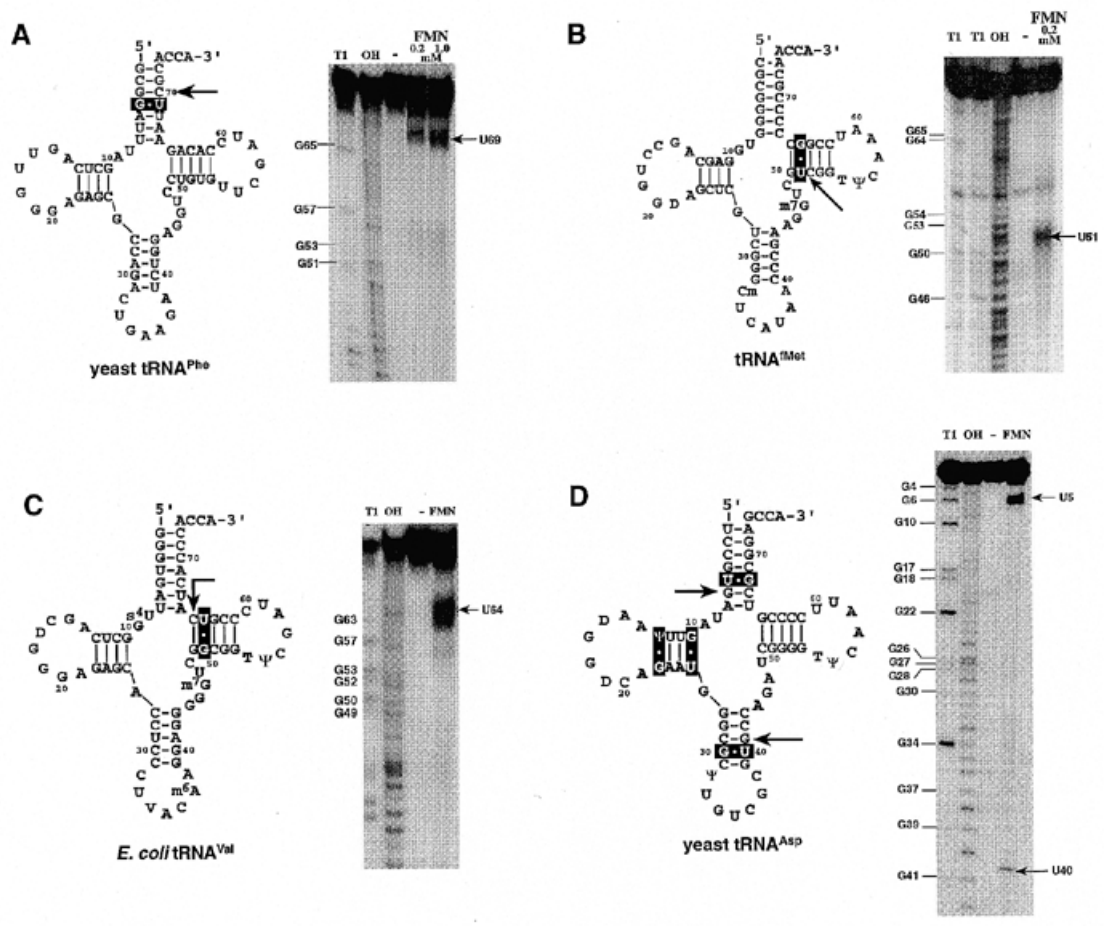

Figure 2. FMN-induced photooxidative cleavage of tRNAs. T1, RNase T1 sequencing ladder; OH, alkaline hydrolysis ladder; –, control incubation for 1 h at 25°C in cleavage buffer with light irradiation without FMN; FMN, incubation with 200 μM FMN for 1 h at 25°C in cleavage buffer with light irradiation. Cleavage sites are indicated by arrows, G·U and GΨ base pairs are highlighted by the black boxes. (**A**) Secondary structure of yeast $tRNA^{Phe}$ and FMN-induced cleavage pattern of 5′-^{32}P-end labeled yeast $tRNA^{Phe}$. The cleavage site is indicated by the arrow, the G·U base pair is highlighted by the black box (10). (**B**) Secondary structure of yeast $tRNA^{fMet}$ and FMN-induced cleavage pattern of 5′-^{32}P-end-labeled yeast $tRNA^{fMet}$ (10). (**C**) Secondary structure of yeast $tRNA^{Val}$ and FMN-induced cleavage of 5′-end-labeled yeast $tRNA^{Val}$. (**D**) Secondary structure of yeast $tRNA^{Asp}$ and FMN-induced cleavage pattern of 3′-^{32}P-end-labeled yeast $tRNA^{Asp}$. The minor cleavage signal corresponds to the [3′-^{32}P]pCp-labeled cleavage fragment at G30·U40.

The finding that no bias for the nucleoside removed exists and that cleavage site selection is directed by a G·U base pair significantly differs from the sequence specificity observed in photosensitized DNA cleavage and indicates that it is the ribose moiety rather than the base which is attacked during cleavage. Treatment of dsDNA with photosensitizers, including Ru(III) intercalators (40,41), were found to affect mainly guanine residues. With flavins DNA cleavage was observed only after incubation with piperidine (7) and mechanisms in which the photosensitizer directly or indirectly destroys the base have been suggested (5). A non-endogenous synthetic system consisting of an isoalloxazine ring covalently attached to either netropsin (8) or distamycin (42) resulted in a single-strand break in dsDNA upon irradiation with visible light. In this cleavage mechanism an attack at the deoxyribose induced by the irradiated isoalloxazine moiety has been discussed. Sequence specificity for A:T-rich regions was observed which resulted, however, from the attached groove binders.

Photocleavage requires isoalloxazine and divalent metal ions

To compare the activity of different isoalloxazine derivatives in the cleavage reaction, RNAs were incubated with FMN, riboflavin, lumiflavin (Fig. 3A), FAD or lumichrome. In addition, to test for a requirement for divalent metal ions, the reaction was performed in the presence and absence of magnesium. As expected, the non-photosensitizing FAD and lumichrome were inactive in strand scission (data not shown; FAD is non-photosensitizing because at pH 7.6 the adenosine is stacked onto the flavin ring and quenches the excited triplet state; 43). With the other isoalloxazine derivatives no significant difference in activity was observed, although isoalloxazine exhibited a slightly higher activity than FMN and riboflavin. Quantification of the band at the G68·U5 base pair revealed >10% cleavage of the total input RNA after 1 h.

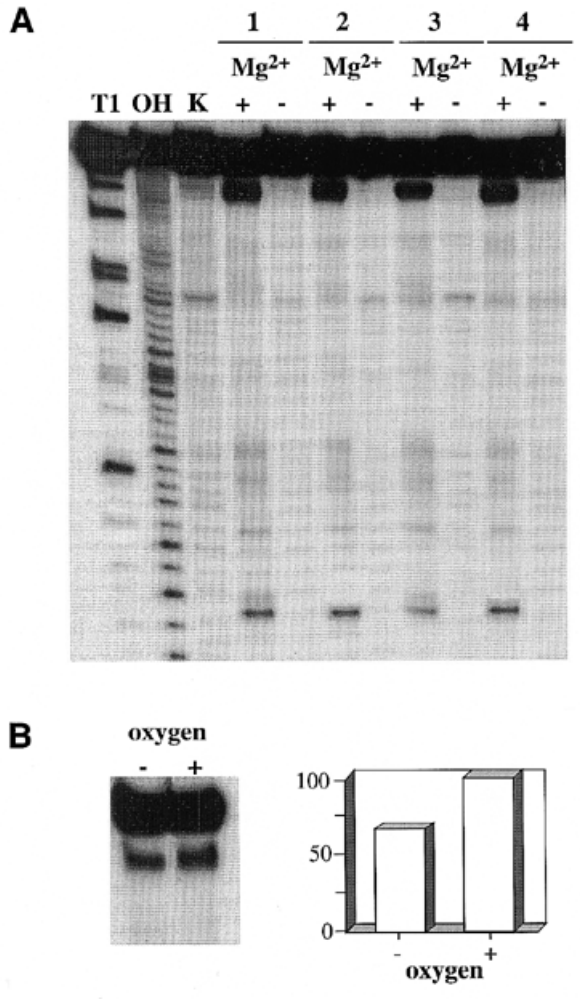

Figure 3. (**A**) Cleavage of $tRNA^{Asp}$ with different isoalloxazine derivatives in the presence and absence of Mg^{2+}. T1, RNase T1 sequencing ladder; OH, alkaline hydrolysis ladder; K, control incubation for 1 h at 25°C in cleavage buffer with light irradiation without photosensitizer; 1, 200 μM FMN with 10 mM Mg^{2+} (+) and without divalent cation (–); 2, as 1 with 200 μM riboflavin; 3, as 1 with 100 μM FMN; 4, as 1 with 100 μM lumiflavin. In a typical cleavage assay 200 μM isoalloxazine derivative was used. For lumiflavin, however, a 100 μM final concentration had to be used because of reduced solubility of this compound in the cleavage buffer. For comparison, a cleavage reaction with 100 μM FMN was done in parallel. (**B**) Cleavage of tRN^{Asp} in the presence and absence of oxygen.

For cleavage to occur, the presence of divalent metal ions is absolutely required, independent of the photosensitizer molecule used. In the presence of divalent metal ions, such as Mg^{2+}, Ca^{2+}, Sr^{2+}, Ba^{2+}, Zn^{2+} and Cd^{2+}, the reaction proceeds equally efficiently. On the other hand, Mn^{2+} and Cu^{2+} are unable to mediate cleavage (data not shown), presumably because these metals are triplet state quenchers (44). The requirement for divalent metal ions was confirmed in cleavage reactions performed with other RNAs, including synthetic oligoribonucleotides (10; Table 1). The photocleavage reaction was also tested at different concentrations of divalent metal ions and was found to occur equally well at concentrations above 1.0 mM. All reactions contained 250 mM Na^+, but cleavage still proceeds well when Na^+ is omitted from the buffer, showing that the reaction does not require monovalent metal ions. The requirement for divalent metal ions for the flavin-dependent RNA cleavage found here contrasts with a study reporting radical-induced cleavage of RNA by Fe(II)-bleomycin (33) at the major cleavage sites A31 and G53 of $tRNA^{Phe}$. This cleavage reaction only takes place in the absence of Mg^{2+} ions.

As demonstrated previously, the photocleavage reaction occurs via an oxidative cleavage process rather than by a hydrolytic mechanism (10). Mechanisms of photosensitization can be divided into two classes; in type I reactions the triplet state photosensitizer interacts directly with the target molecule by either abstraction or donation of electrons or H atoms. In some cases the resulting substrates react with oxygen to give oxidized products of various types (43). In type II mechanisms the excited photosensitizer interacts with ground state oxygen to generate a singlet oxygen molecule, $^1O_2$, which can readily react with electron-rich regions of many biomolecules to yield oxidized species (43). Figure 3B demonstrates that the cleavage reaction also occurs in the absence of oxygen, albeit with 30–40% reduced activity, indicating that the effect might occur via a photosensitizer type I mechanism. Riboflavin is an effective photosensitizer of the guanine moiety in DNA, acting predominantly through a type I mechanism (45). In accordance with a type I mechanism, Kasai *et al*. have shown that formation of 7,8-dihydro-8-oxo-2′-deoxyguanosine (8-hydroxy-2′-deoxyguanosine) after treatment of dsDNA with riboflavin occurs by a mechanism which does not involve participation of any reactive oxygen species (6).

G·U base pairs affected in the td intron

We used our new structure probing technique based on the photooxidative targeting of G·U base pairs to map G·U base pairs in the precursor RNA of the T4 phage-derived thymidylate synthase (td) intron (16; Fig. 4). The 265 nt group I intron contains several G·U base pairs located within stems or as closing base pairs of loops, as shown in the secondary structure model in Figure 4A. This intron belongs to subgroup IA2, as does the T4 nrdD intron, which was previously characterized physicochemically and for which a 3-dimensional model exists (17). Gel separation of the 5′-labeled intron reveals a major site of cleavage 3′ of U102, which forms a base pair with G90, and two minor cleavage sites downstream of U72·G53 and U93·G99 (Fig. 4B). Two other strong bands are visible in the region close to the 3′-end which were resolved by analyzing the 3′-end-labeled intron RNA. Analysis confirmed that these two additional cleavages occur at G141·U152 and G235·U253, located in stems P7.2 and P9.2 respectively. The second G233·U255 pair of stem 9.2, located at a helix extremity, was not affected. Furthermore, no cleavage could be detected in stem P1, which contains two sets of tandem G·U pairs (Fig. 4C). As shown in Figure 4C, a low percentage of spontaneous magnesium-dependent hydrolysis at the 5′-splice site of the td intron is detected under the reaction conditions used in this study, indicating that P1 is correctly positioned on the catalytic core under our experimental conditions and that the intron is folded in an active conformation. An experimental indication of correct docking of stem P1 is site-specific hydrolysis at the 5′-splice site by Mg^{2+}, resulting in products similar to guanosine-dependent splicing (31,46). The cleavage pattern for the td intron is summarized in Table 2.

Some G·U pairs located at a helical extremity are not affected by isoalloxazine-induced photocleavage whereas others are

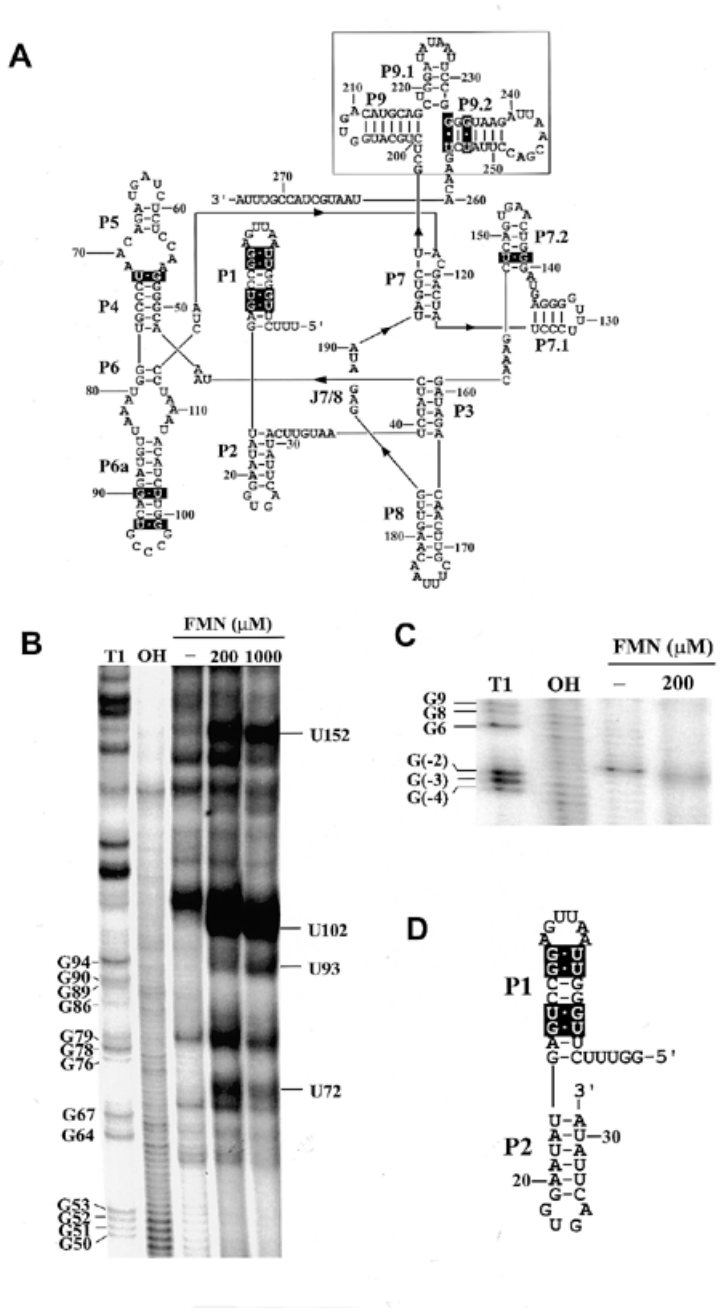

Figure 4. G·U pairs affected in the td intron and a synthetic construct resembling P1 and P2. (**A**) Secondary structure and stem numbering scheme of the td intron. All G·U base pairs are highlighted by a black box. (**B**) Section from a gel showing FMN-induced cleavage with cuts at U72, U93, U102 and U152 of the 5′-^{32}P-end-labeled td intron. (**C**) Section from a gel showing spontaneous, magnesium-dependent hydrolysis at the 5′-splice site of the 5′-^{32}P-end-labeled td intron. No difference in the intensities of the band corresponding to hydrolysis at U1 with or without FMN was measured. T1, RNase T1 sequencing ladder; OH, alkaline hydrolysis ladder. Cleavage conditions were the same as in other experiments described for the td intron. (**D**) Sequence of the synthetic P1/P2 construct.

affected. For example, U72·G53 and U93·G99 in the td intron, both located at the helical extremities of stems P4 and P6a respectively, show a weak, but clearly detectable cleavage band, whereas the Ψ13·G22 and G10·U25 base pairs in tRNA^{Asp} and the G233·U255 wobble in P9.2 in the td intron do not yield a cleavage signal. We do not think that the presence of a pseudouridine is the reason for the lack of cleavage at that position. However, in the crystal structure (14,15) the Ψ13·G22 base pair stacks with the *trans* Hoogsteen tertiary base pair A14·U8 with a twist angle between the two base pairs of ~90°. Similarly, but to a lesser extent, the twist angle at the junction between the D helix and the AC helix, i.e. G10·U25 and G26·A44, is ~45°. These examples show that for cleavage to occur the twist angle between the G·U base pair and the 3′ base pair should be close to the standard 33° of A-form RNA helices. Thus, one would conclude that the helical stacking is maintained 3′ of U72·G53 and U93·G99. At a helical extremity the binding surface for FMN is reduced, preventing FMN from binding to RNA and thus explaining the lack of cleavage at such positions (see below).

Table 2. FMN-dependent cleavage at G·U pairs in the td intron and the synthetic P1 construct

G·U pair	Residue 3′ of U	Intensity
td intron		
U(–5)–G13		–
G(–4)–U12		–
U(–1)–G9		–
U1–G8		–
G53–U72	C	+
G90–U102	C	++
U93–G99	C	+
G141–U152	C	++
G233–U255		–
G235–U253	C	++
P1 construct[a]		
U(–5)–G13		–
G(–4)–U12		–
U(–1)–G9		–
U1–G8		–

[a]The P1 construct was tested in parallel at 12, 30, 50, 70 and 100 mM Mg^{2+} at 23°C as well as at 4°C. In no case was cleavage observed.

How might the lack of cleavage activity for the two sets of tandem G·U pairs in stem P1 be explained? The most likely explanation for lack of cleavage in the P1 stem would be that tandem G·U pairs alter the binding site for the isoalloxazine ring so that recognition by the isoalloxazine moiety becomes weaker or impossible. Alternatively, the G·U pairs of the P1 stem in the td intron might not be accessible to the FMN probe because the stem is docked onto the catalytic core of the intron (as indicated by spontanous hydrolysis at the splice site; see Fig. 4C). To test this, we synthesized a 48mer truncated version of the intron containing nt –10 to 31, including stems P1 and P2 (Fig. 4D and Table 2), and subjected it to isoalloxazine cleavage under the same conditions as the td intron. As in the full-length intron, no cleavage at the two sets of tandem G·U pairs was observed. The same negative result was obtained when the cleavage reaction was performed at 30, 50, 70 and 100 mM Mg^{2+} at 23°C as well as 4°C (Table 2). This result indicates that the lack of cleavage at the two tandem G·U pairs in the P1 stem of the td intron is due to the fact that tandem G·U pairs are cleaved significantly less, if at all, for geometrical reasons rather than to the fact that they are not accessible. Indeed, a comparison of crystal structures (see below) indicates that in tandem G·U pairs the sugar moiety forming part of the binding surface for FMN is moved towards the binding position of the dimethyl isoalloxazine ring, preventing it from binding to the RNA.

In agreement with the refined secondary structure (17), in which the P9 extension is such that C218 is paired with G232 while U219 bulges out and G233 pairs to U255 (see box in Fig. 4A), there is no cleavage at U219 in stem P9.1. Previously, U219 was suggested to pair with G232 forming a G·U pair, while C218 was paired with G233 extending stem P9.1 by an additional base pair (47). Together, these observations constitute an independent confirmation of the phylogenetically and experimentally derived secondary structure (17) and demonstrate the power of photo-oxidative flavin-dependent cleavage as a probe for establishing fine structural details in RNAs.

Minor cleavages at other sites

While the overwhelming majority of cuts observed in the RNAs used in this study occur at G·U base pairs, very weak cuts at positions which do not correspond to a G·U base pair were detected in two instances: G50·C63 in $tRNA^{Asp}$ and at the second G in a GGGA loop of a hairpin construct (data not shown). Presently, on the basis of the available data, we cannot explain these weak cuts. The only structural property common to the regions where these cuts occur is that the sugar–phosphate backbone folds back on itself with a sharp turn bringing two or more phosphate groups close to each other. Accordingly, a possible explanation might be that in such negatively charged and open pockets magnesium binding is facilitated while, at the same time, another type of stacking of the isoalloxazine ring, such as intercalation, would be permitted. Further experiments aimed at a better understanding of these weak cuts are under way.

A model for G·U recognition

The specificity of the cleavage reaction for G·U base pairs suggests that the isoalloxazine ring specifically recognizes geometrical and structural features resulting from the presence of a G·U pair within a helical region. It is likely that the isoalloxazine enters its G·U recognition site from the shallow groove of the helix. Indeed, the 3′-end of the paired U is readily accessible since in G·U wobble pairs the uracil base points into the deep groove of the RNA helix, forming a hollow surface within the shallow groove. Such cavities are often a site of specific hydration in RNAs, with the occupying water molecule either bridging the two bases of the G·U pair or the O2(U) and O2′(U) (39,48). A structural model illustrating a possible complex between an RNA helix containing a G·U pair, FMN and a magnesium ion is presented in Figure 5A. The model is based on coordinates (15) of the acceptor stem helix of yeast $tRNA^{Asp}$. The binding of FMN exploits the shallow groove asymmetry of G·U pairs by inserting the FMN exocyclic O2 atom in the space left by the presence of the uracil instead of a cytosine. Two hydrogen bonds from FMN to the RNA are suggested by the model, namely to the amino group of the guanine and to the 2′-OH of the uridine within the G·U pair (Fig. 5A). In order to account for the magnesium requirement in isoalloxazine cleavage, a Mg^{2+} ion was intially placed as a bridge between O4 of FMN and the phosphate group 3′ of the uracil residue. However, molecular dynamics simulations (Fig. 5B; see also below) performed on the model of the complex suggested that there is an additional water molecule involved in this bridging interaction. The aromatic isoalloxazine ring stacks on the flat surface constituted by the sugar 3′ of the uridine. Thus, the N5 atom of FMN, which carries the excited triplet orbital, is positioned close above the H1′ and H4′ atoms of the cleaved residue, either of which could be attacked during the cleavage reaction (10). Sugar ring opening might result from hydrogen abstraction, from either the C4′ or the C1′ atom (49). For steric and accessibility reasons the C4′ atom is more susceptible to attack than C1′. Abstraction of H4′ would be in accordance with oxidative cleavage mechanisms commonly found in DNA cleavage reactions (49) induced, for example, by

copper-phenanthroline (50), enediines (51), bleomycin (52), Fe-EDTA and Fe-MPE (53). It should be noted, however, that the cleavage mechanism might involve an electron transfer step rather than hydrogen abstraction.

As summarized in Table 1, all G·U pairs within a helix are cleaved (10). Uncleaved or poorly cleaved bases 3′ of the U residues (see also Table 2) occur when the G·U pair is located at a helical extremity, a structural situation which removes the extended flat surface on which the isoalloxazine ring binds. Similarly, a movement of the sugar 3′ of the U is probably responsible for the observed lack of cleavage activity found for tandem G·U pairs. Superimposition of an isolated G·U pair of one such tandem array from the $tRNA^{Asp}$ acceptor stem on such pairs within G·U/G·U or G·U/U·G doublets(54) shows that due to an increased base pair twist angle the sugar 3′ of the U moves towards the normal binding position of the isoalloxazine ring (Fig. 6). Thus, the FMN could probably not engage at the same time in the two interactions necessary for binding to RNA, namely hydrogen bonding to the G·U pair and stacking on the sugar moiety 3′ of U.

In order to assess the stability of the model, we performed molecular dynamics simulations (Fig. 7) under the most sophisticated conditions on a fully hydrated and neutralized RNA–FMN complex in a periodic system using Ewald summation for correct treatment of electrostatic interactions. During the simulations the FMN stayed close to its starting position and the two essential hydrogen bonds between FMN and the RNA remained intact (data not shown). Additional hydrogen bonding was observed between one of the hydroxyl groups of the FMN sugar moiety and the RNA backbone (Fig. 5B). The Mg^{2+} ion did not stay at its starting position, where it directly bridges FMN and the RNA. After rearrangement of the hydration structure around the Mg^{2+} ion a stable geometry was reached where O4 of FMN interacts with the Mg^{2+} ion via an additional water molecule (Fig. 5B). This suggests that the magnesium ion may be more important for the cleavage chemistry rather than for the structure of the complex. Most importantly, the reactive nitrogen atom N5 of FMN remained within close proximity to the attacked H4′ atom in the RNA (Fig. 7). As a control, we constructed a second model where the isoalloxazine ring was flipped about its long axis, conserving the proximity of N5 to the attacked H4′ atom. The interaction of H3 with the 2′-OH of the uridine remained the same as in the first model while the partners of O2 and O4 were exchanged (O4 to guanine, O2 to magnesium). During molecular dynamics simulations of this alternative FMN–RNA complex we observed dissociation of FMN from the RNA. The hydrogen bonds to the RNA did not remain stable (Fig. 7B). Thus, we conclude that the first complex (Fig. 5A) represents a stable mode of FMN binding to RNA.

Clearly, the experimental data do not give specific information on water molecules and magnesium coordination, which must await a crystal structure. However, the simulations yield a

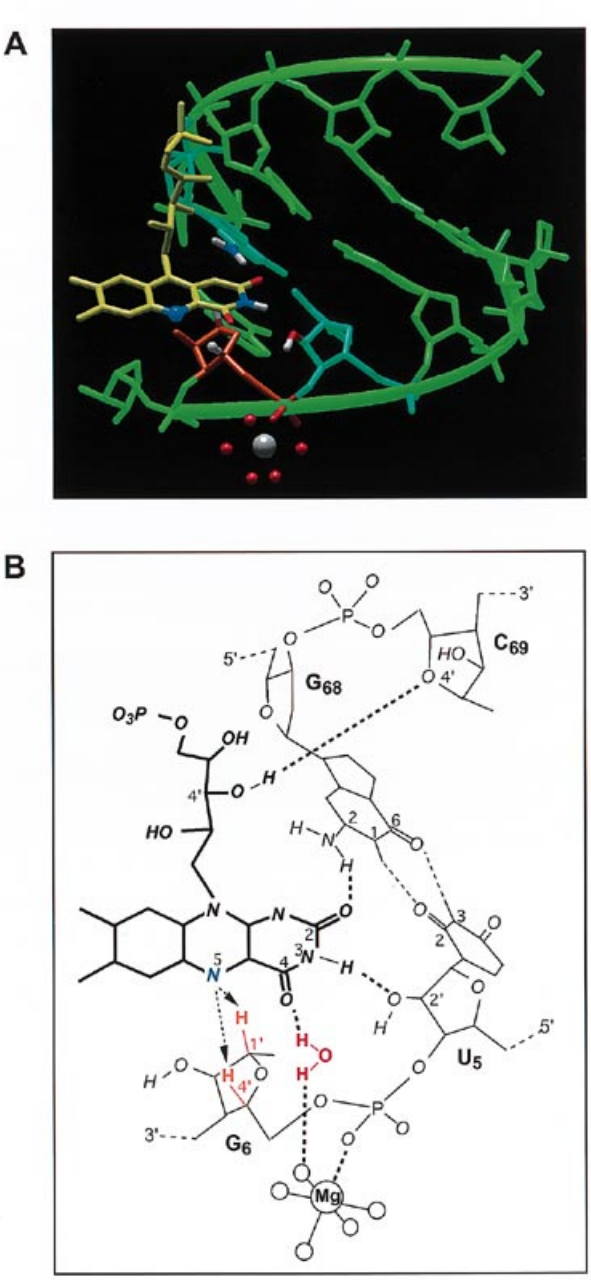

Figure 5. The modeled FMN–RNA complex. (**A**) Stick representation of the modeled complex between the $tRNA^{Asp}$ acceptor stem (green) with the U5·G68 base pair (light blue) and FMN (yellow). The sugar of the nucleotide 3′ of the U that carries the reactive hydrogen atoms H1′ and H4′ is colored orange. This sugar moiety also provides the flat surface for binding of the FMN ring system. The H1′ and H4′ atoms (white) are marked with balls, along with the N5 atom (blue), which is the reactive center of FMN. The carbonyl oxygen attached to C2 was positioned where a water molecule is frequently observed in crystal structures containing G·U base pairs so that a hydrogen bond to the N2 amino group of the paired guanine is possible. The imino hydrogen bound to nitrogen N3 is oriented so as to form a hydrogen bond to the O2′ atom of U5 (red) (see B). Note also the close contact of the FMN N5 atom to the hydrogen attached to the C1′ and C4′ atoms of G6, which should undergo hydrogen abstraction with subsequent opening of the ribose ring and removal of the nucleotide. The magnesium ion bound to the phosphate 5′ of G6 does not form a direct contact to the isoalloxazine ring (see B). (**B**) Interactions between FMN and the RNA in the modeled complex. Hydrogen bridges are shown as dashed lines. A probable interaction between N5, the reactive center of FMN, and the hydrogen atoms attacked, H1′ or H4′ of G6, is indicated by dashed arrows. The G·U pair provides two hydrogen bonds, namely one on the G sidechain to a carbonyl group in FMN and one on the U backbone 2′-OH group to the amide group in FMN. During molecular dynamics simulations an additional hydrogen bond is formed between a hydroxyl group of the FMN sugar moiety and the 4′O atom of C69. A contact mediated via a bridging water molecule is observed between FMN and the hydration shell of the magnesium ion bound to the phosphate of G6.

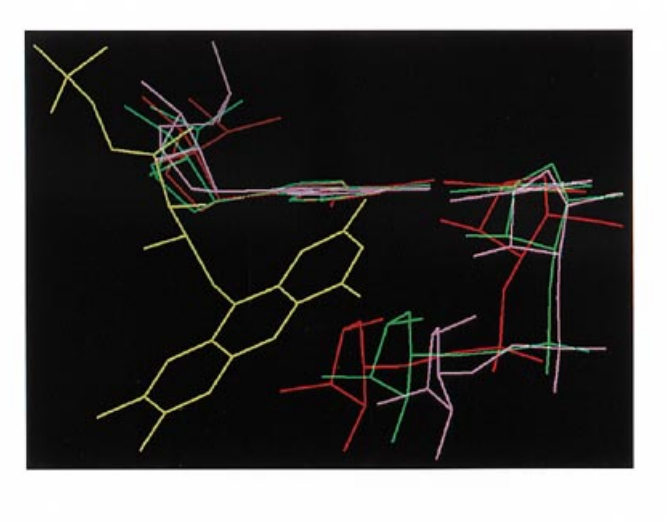

Figure 6. Comparison of the position of the sugar moiety 3′ of the uridine for different G·U pairs. The structure of the G·U pair from the modeled complex obtained by averaging over 50 conformations during molecular dynamics simulation is shown in green. FMN is yellow. The structure of a G·U pair within tandem G·U pairs in P1, from the crystal structure of the td intron, is in red (54). The structure of the G10·U25 base pair in $tRNA^{Asp}$ is shown in magenta. In both cases, i.e. the tandem G·U pairs in P1 of the td intron and the G10·U25 base pair in $tRNA^{Asp}$, FMN cleavage is absent. In the tandem G·U pairs the sugar moiety that forms the surface for binding of FMN is moved towards the binding position of FMN. In the G10·U25 base pair in $tRNA^{Asp}$ this sugar moiety is retracted. Obviously, both kinds of deviations of the sugar moiety position 3′ of the uridine prevent FMN from binding to RNA.

plausible model for the complex between a G·U pair and a FMN molecule in which the interactions with water molecules and magnesium ions occupy positions energetically favorable and stable within the framework of the AMBER 4.1 forcefield. The model consistently rationalizes all the cleavage data obtained in this study.

Conclusion

Our results show that RNA cleavage by the isoalloxazine ring depends on a molecular recognition event relying on the geometry and structure at G·U base pairs. Based on molecular dynamics simulations, we present an energetically stable 3-dimensional model illustrating the ternary complex of the G·U-containing helical stack, the isoalloxazine molecule and the metal ion which rationalizes the cleavage specificity along with the experimental data. As it is well established that RNA structures contain various different non-canonical base pairs (55,56), many of which are proven to also be present in the RNAs tested in this study, the specificity of cleavage site selection by the photosensitizer isoalloxazine for an individual class of non-canonical base pairs is striking. This photocleavage reaction thus opens up the interesting possibility of probing, in folded RNAs, the accessibility of G·U base pairs embedded within helices, which are known to be endowed with specific structural and functional roles in numerous structured and catalytic RNAs and interactions of RNA with proteins.

Remarkably little is known about specificity and even activity of photosensitizer-induced RNA cleavage. The only known example showing that RNAs are affected by photosensitizers is psoralen-induced photocrosslinking (57) of various positions in

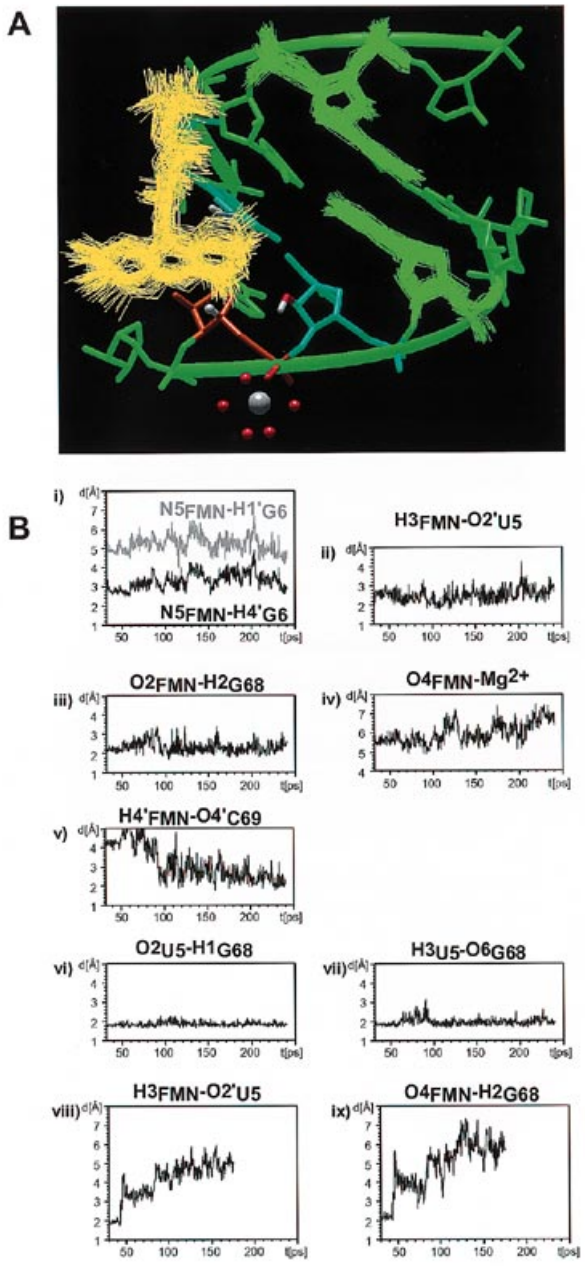

Figure 7. Results of the molecular dynamics simulations performed on the FMN–RNA complex. (**A**) Dynamic behavior of the FMN bound to RNA. Fifty conformations of FMN (yellow) obtained during 200 ps productive simulation at 298 K are shown in an overlay plot on a stick model of the RNA. For comparison the dynamic behavior of the RNA is depicted for two selected nucleotides (green). The color scheme is the same as in Figure 5A. (**B**) Recording of interatomic distances during a representative simulation (see also Fig. 5): (i) distances between the reactive center of FMN (N5) and the hydrogen atoms attacked in the RNA (H1′ and H4′ of G6); (ii and iii) distances between hydrogen bond donors and acceptors in the interaction between FMN and the G·U pair (H3FMN to O2′U5 and O2FMN to H2G68); (iv) distance between the FMN carbonyl group at position 4 and the Mg^{2+} ion; (v) bond length of a newly formed hydrogen bond between the sugar moiety of FMN and the RNA; (vi and vii) for comparison, the hydrogen bond lengths within the G·U pair; (viii and ix) the same distances as in (ii) and (iii) for a second simulation with an alternative FMN–RNA complex model that was not stable during simulations.

rRNAs, tRNAs and the spliceosome. The photoreaction of psoralens with RNA, however, occurs via a completely different mechanism than the cleavage mechanism described here. In addition to its potential application as a specific structural probe, the endogenous biological cofactor riboflavin may be a cheap and innocuous candidate to be tested for biomedical applications such as photochemical inactivation of RNA viruses in contaminated blood plasma and vaccines.

NOTE ADDED IN PROOF

The following paper came to our attention in which a similar effect was observed with Tris(4,7-diphenyl-1,10-phenanthroline) rhodium(III) using UV photocleavage: Chow,C.S. and Barton, J.K. (1992) *Biochemistry*, **31**, 5423–5429.

ACKNOWLEDGEMENTS

We thank R.Schroeder for the generous gift of the plasmid td ΔP6-2T, G.Keith for samples of $tRNA^{Asp}$, F.Michel, W.Kolanus and D.Faulhammer for helpful discussions and E.-L.Winnacker for support. This study was supported in part by grants from the Deutsche Forschungsgemeinschaft to M.F. and an EC grant (Bio2CT930345) to M.F. and E.W. T.H. is supported by an EMBO post-doctoral fellowship.

REFERENCES

1 Shibutani,S., Takeshita,M. and Grollman,A.P. (1991) *Nature*, **349**, 431–434.
2 Diwu,Z. and Lown,J.W. (1994) *Pharmacol. Ther.*, **63**, 1–35.
3 Diamond,I., McDonagh,A.F., Wilson,C.B., Granelli,S.G., Nielsen,S. and Jaenicke,R. (1972) *Lancet*, **ii**, 1175–1177.
4 Hanson,C.V. (1983) *Medical Virology*. Elsevier, Amsterdam, The Netherlands, Vol. 2, pp. 45–79.
5 Buchko,G.W., Cadet,J., Berger,M. and Ravanat,J.-L. (1992) *Nucleic Acids Res.*, **20**, 4847–4851.
6 Kasai,H., Yamaizumi,Z., Berger,M. and Cadet,J. (1992) *J. Am. Chem. Soc.*, **114**, 9692–9694.
7 Ito,K., Inoue,S., Yamamoto,K. and Kawanishi,S. (1993) *J. Biol. Chem.*, **268**, 13221–13227.
8 Bouziane,M., Ketterle,C., Helissey,P., Herfeld,P., Le Bret,M., Giorgi-Renault,S. and Auclair,C. (1995) *Biochemistry*, **34**, 14051–14058.
9 Burgstaller,P. and Famulok,M. (1994) *Angew. Chem. Int. Edn English*, **33**, 1084–1087.
10 Burgstaller,P. and Famulok,M. (1997) *J. Am. Chem. Soc.*, **119**, 1137–1138.
11 Hingerty,B., Brown,R.S. and Jack,A. (1978) *J. Mol. Biol.*, **124**, 523–534.
12 Ladner,J.E. and Klug,A. (1975) *Proc. Natl. Acad. Sci. USA*, **72**, 4414–4418.
13 Sussman,J.L., Holbrook,S.R., Warrant,R.W., Church,G.M. and Kim,S.H. (1978) *J. Mol. Biol.*, **123**, 607–630.
14 Westhof,E., Dumas,P. and Moras,D. (1985) *J. Mol. Biol.*, **184**, 119–145.
15 Westhof,E., Dumas,P. and Moras,D. (1988) *Acta Crystallogr.*, **44A**, 112–123.
16 Chu,F.K., Maley,G.F., Maley,F. and Belfort,M. (1984) *Proc. Natl. Acad. Sci. USA*, **81**, 3049–3053.
17 Jaeger,L., Westhof,E. and Michel,F. (1993) *J. Mol. Biol.*, **234**, 331–346.
18 Strobel,S.A. and Cech,T.R. (1995) *Science*, **267**, 675–679.
19 Michel,F., Umesono,K. and Ozeki,H. (1989) *Gene*, **82**, 5–15.
20 Abramovitz,D.L., Friedman,R.A. and Pyle,A.M. (1996) *Science*, **271**, 1410–1413.
21 Pyle,A.M., Moran,S., Strobel,S.A., Chapman,T., Turner,D.H. and Cech,T.R. (1994) *Biochemistry*, **33**, 13856–13863.
22 Knitt,D.S., Narlikar,G.J. and Herschlag,D. (1994) *Biochemistry*, **33**, 13846–13879.
23 Musier-Forsyth,K., Usman,N., Scaringe,S., Doudna,J., Green,R. and Schimmel,P. (1991) *Science*, **253**, 784–786.
24 Moore,M.J., Query,C.C. and Sharp,P.A. (1993) In Gesteland,R.F. and Atkins,J.F. (eds), *The RNA World*. Cold Spring Harbor Laboratory Press, Cold Spring Harbor, NY, pp. 303–357.
25 Gutell,R.R., Larsen,N. and Woese,C.R. (1994) *Microbiol. Rev.*, **58**, 10–26.
26 McClain,W.H., Gabriel,K. and Schneider,J. (1996) *RNA*, **2**, 105–109.
27 Streicher,B., Von Ahsen,U. and Schroeder,R. (1993) *Nucleic Acids Res.*, **21**, 311–317.
28 Davanloo,P., Rosenberg,A.H., Dunn,J.J. and Studier,F.W. (1984) *Proc. Natl. Acad. Sci USA*, **81**, 2035–2039.
29 Geiger,A., Burgstaller,P., Von der Eltz,H., Roeder,A. and Famulok,M. (1996) *Nucleic Acids Res.*, **24**, 1029–1036.
30 Schroeder,R., Von Ahsen,U. and Belfort,M. (1991) *Biochemistry*, **30**, 3295–3303.
31 Streicher,B., Westhof,E. and Schroeder,R. (1996) *EMBO J.*, **15**, 2556–2564.
32 Donis-Keller,H., Maxam,A.M. and Gilbert,W. (1977) *Nucleic Acids Res.*, **4**, 2527–2538.
33 Hüttenhofer,A., Hudson,S., Noller,H.F. and Mascharak,P.K. (1992) *J. Biol. Chem.*, **267**, 24471–24475.
34 Hüttenhofer,A. and Noller,H.F. (1992) *Proc. Natl. Acad. Sci. USA*, **89**, 7851–7855.
35 Cornell,W.D., Cieplak,P., Bayly,C.I., Gould,I.R., Merz,K.M., Ferguson,D.M., Spellmeyer,D. C., Fox,T., Caldwell,J.W. and Kollman,P.A. (1995) *J. Am. Chem. Soc.*, **117**, 5179–5197.
36 Hermann,T. and Heumann,H. (1995) *RNA*, **1**, 1009–1017.
37 Åqvist,J. (1990) *J. Phys. Chem.*, **94**, 8081–8024.
38 Auffinger,P. and Westhof,E. (1996) *Biophys. J.*, **71**, 940–954.
39 Auffinger,P. and Westhof,E. (1997) *J. Mol. Biol.*, **269**, 326–341.
40 Arkin,M.R., Stemp,E.D.A., Coates Pulver,S. and Barton,J.K. (1997) *Chem. Biol.*, **4**, 389–400.
41 Stemp,E.D.A., Arkin,M.R. and Barton,J.K. (1997) *J. Am. Chem. Soc.*, **119**, 2921–2925.
42 Herfeld,P., Helissey,P., Giorgi-Renault,S., Goulaouic,H., Pager,J. and Auclair,C. (1994) *Bioconjugate Chem.*, **5**, 67–76.
43 Spikes,J.D. (1989) In Smith,K.C. (ed.), *The Science of Photobiology*, 2nd Edn. Plenum Press, New York, NY, pp. 79–110.
44 Hemmerich,P. and Lauterwein,J. (1973) In Eichhorn,G. (ed.), *Inorganic Biochemistry*, 2nd Edn. Elsevier, Amsterdam, The Netherlands.
45 Midden,W.R. and Wang,S.J. (1983) *J. Am. Chem. Soc.*, **105**, 4129–4135.
46 Inoue,T., Sullivan,F.X. and Cech,T.R. (1986) *J. Mol. Biol.*, **189**, 143–165.
47 Belfort,M., Chandry,P.S. and Pedersen-Lane,J. (1987) *Cold Spring Harbor Symp. Quant. Biol.*, **52**, 181–192.
48 Westhof,E. (1988) *Annu. Rev. Biophys. Biophys. Chem.*, **17**, 125–144.
49 Pratviel,G., Bernadou,J. and Meunier,B. (1995) *Angew. Chem. Int. Edn English*, **34**, 746–770.
50 Kuwabara,M., Yoon,C., Goyne,T., Thederahn,T. and Sigman,D.S. (1986) *Biochemistry*, **25**, 7401–7408.
51 Kappen,L.S. and Goldberg,I.H. (1992) *Proc. Natl. Acad. Sci. USA*, **89**, 6706–6710.
52 Rabow,L.E., McGall,G.H., Stubbe,J. and Kozarich,J.W. (1990) *J. Am. Chem. Soc.*, **112**, 3203–3208.
53 Hertzberg,R.P. and Dervan,P.B. (1984) *Biochemistry*, **23**, 3934–3945.
54 Cate,J.H., Gooding,A.R., Podell,E., Zhou,K., Golden,B.L., Kundrot,C.E., Cech,T.R. and Doudna,J.A. (1996) *Science*, **273**, 1678–1685.
55 Wyatt,J.R. and Tinoco,J.I. (eds) (1993) In Gesteland,R.F. and Atkins,J.F. (eds), *The RNA World*. Cold Spring Harbor Laboratory Press, Cold Spring Harbor, NY, pp. 465–496.
56 Nagai,K. and Mattaj,I.W. (1994) *RNA–Protein Interactions*. Oxford University Press, Oxford, UK.
57 Cimino,G.D., Gamper,H.B., Isaacs,S.T. and Hearst,J.E. (1985) *Annu. Rev. Biochem.*, **54**, 1151–1193.